https://doi.org/10.5194/hess-2019-328
Preprint. Discussion started: 3 July 2019

Hydrology and Earth System Sciences
Discussions

Identifying uncertainties in simulated streamflow from hydrologic model components for climate change impact assessments

Dongmei Feng[1*] and Edward Beighley[2,3]
[1] Civil and Environmental Engineering, University of Massachusetts, Amherst, MA, USA
[2] Civil and Environmental Engineering, Northeastern University, MA, USA
[3] Marine and Environmental Sciences, Northeastern University, MA, USA
[*]Corresponding author, email address: dmei.feng@gmail.com, telephone: (617) 697-8789

Abstract: Assessing the impacts of climate change on hydrologic systems is critical for developing adaptation and mitigation strategies for water resource management, risk control and ecosystem conservation practices. Such assessments are commonly accomplished using outputs from a hydrologic model forced with future precipitation and temperature projections. The algorithms used in the hydrologic model components (e.g., runoff generation) can introduce significant uncertainties in the simulated hydrologic variables, yet the identification and quantification of such uncertainties is rarely studied. Here, a modeling framework is developed that integrates multiple runoff generation algorithms with a routing model and associated parameter optimizations. This framework is able to identify uncertainties from both hydrologic model components and climate forcings as well as associated parameterization. Three fundamentally different runoff generation approaches: runoff coefficient method (RCM, conceptual), variable infiltration capacity (VIC, physically-based, infiltration excess) and simple-TOPMODEL (STP, physically-based, saturation excess), are coupled with Hillslope River Routing model to simulate streamflow. A case study conducted in Santa Barbara County, California, reveals that the median changes are 1-10% increases in mean annual discharge (Q_m) and 10-40% increases in annual maximum daily discharge (Q_p) and 100-yr flood discharge (Q_{100}). The Bayesian Model Averaging analysis indicates that the probability of increase in streamflow can be up to 85%. However, the simulated discharge uncertainties are large (i.e., 230% for Q_m and 330% for Q_p and Q_{100}) with general circulation models (GCMs) and emission scenarios accounting for more than half of the total uncertainty. Hydrologic process models contribute 10-30% of the total uncertainty, while uncertainty due to hydrologic model parameterization is almost negligible (<1%), limiting the impacts of hydrologic model parameter equifinality in climate change impact analysis. This study also provides insights on how to optimize the selection of hydrologic models for projecting future streamflow conditions.

https://doi.org/10.5194/hess-2019-328
Preprint. Discussion started: 3 July 2019

Hydrology and Earth System Sciences Discussions

1. Introduction

Streamflow is essential to humans and ecosystems, supporting human's life and economic activities, providing habitat for aquatic creatures, and exporting sediment/nutrients to coastal ecosystems (Feng et al., 2016;Barnett et al., 2005;Milly et al., 2005). Understanding streamflow characteristics is important for water-resources management, civil infrastructure design and making adaptation strategies for economic and ecological practices (Feng et al., 2019). With economic development and population growth, the emission of greenhouse gas is likely to increase during 21st century (IPCC, 2014). The increase in global surface temperature is projected to exceed 2°C by the end of 21st century even under moderate emission scenarios (e.g., Representative Concentration Pathways, RCPs, 4.5 and 6.0) (IPCC, 2014). Intensified hydro-meteorological processes, altered precipitation forms and patterns, and intensified atmospheric river events and oceanic anomalies (e.g. El Nino events) are projected and likely to causes substantial impacts on hydrologic fluxes (e.g., streamflow) (Barnett et al., 2005;Tao et al., 2011;Dai, 2013;Dettinger, 2011;Vicky et al., 2018;Cai et al., 2014;Feng et al., 2019).

The integration of climate projections and hydrologic models enables the investigation of streamflow dynamics under the future climate conditions. However, the simulated streamflow contains uncertainties from various sources. Due to epistemic limitations (e.g., human's lack of knowledge about hydrologic processes and boundary conditions) and the complexities in nature (e.g., temporal and spatial heterogeneity), hydrologic models are simplified representations of natural hydrologic processes (Beven and Cloke, 2012). Generally, hydrologic models have modules simulating atmosphere-land interactions associated with water and energy partitioning (named as runoff generation process in this study), and modules simulating the water transportation along terrestrial hillslopes and channels (named as routing process here). Each process can be represented in different ways, which thus results in uncertainties in simulated streamflow. For the runoff generation process, surface runoff is mainly represented as infiltration excess overland flow (or Hortonian flow (Horton, 1933)) or saturation excess overland flow. Infiltration excess overland flow occurs when water falls on the soil surface at a rate higher than that the soil can absorb. Saturation excess overland flow occurs when precipitation falls on completely saturated soils. In addition, surface runoff can also be quantified conceptually, for example, a runoff coefficient can be used to generate surface runoff as a proportion of precipitation

Hydrology and Earth System Sciences
Open Access
EGU
Discussions

rate. Subsurface runoff is generally represented as functions of soil characteristics and topographic features. The complexity of these functions varies significantly, from simple linear to combinations of multiple non-linear. The lateral routing processes are generally represented using various approximations of the Saint-Venant equations (Reed et al., 2004). Difference choices of these process models may achieve different results and thus cause uncertainties in outputs. Parameterization can be another uncertainty source. Due to the nonlinearity of hydrologic processes, different combinations of model parameters can achieve similar, if not identical, model performance. Model parameter selections based on statistical metrics obtained from calibration can result in different optimal parameter values (i.e., parameter equifinality). When it comes to hydrologic impact assessments, the model forcings, which differ among General Circulation Models (GCMs) due to the model discrepancy and the uncertainty of future emission scenarios, also contribute to the uncertainties in simulated streamflow. Without appropriate assessment of these uncertainties, standalone studies on the climate change impacts, using a particular hydrologic model forced by select GCMs' projections under some emission scenarios, can be difficult to interpret. Systematic assessments of the relevant uncertainties associated with simulated streamflow are needed.

Some studies have been performed considering the above at both regional and global scales (for example, (Wilby and Harris, 2006;Vetter et al., 2015;Valentina et al., 2017;Kay et al., 2009;Eisner et al., 2017;Su et al., 2017;Schewe et al., 2014;Hagemann et al., 2013;Asadieh and Krakauer, 2017)). Most previous studies integrated multiple hydrologic models individually. However, the hydrologic model structures can be significantly different, which may limit the ability to quantify relative uncertainty contributions from different model components (e.g., runoff generation model and routing model) and associated parametrizations. Troin et al. (2018) tested the impacts by using different hydrologic model components to simulate streamflow, but they only focused on snow and potential ET methods. In this study, a consistent hydrologic modeling framework that integrates multiple runoff generation process models with surface, subsurface and channel routing processes and associated parameter uncertainties is developed. This framework enables uncertainties from different components representing hydrologic processes and associated model parameters as well as model forcings (e.g., precipitation and temperature) to be quantified and compared in a consistent manner. In this framework, three runoff generation process models which represent the three fundamentally different approaches mentioned above are used. The

https://doi.org/10.5194/hess-2019-328
Preprint. Discussion started: 3 July 2019

conceptual frameworks are adapted from the variable infiltration capacity model (Wood et al., 1992;Liang et al., 1996) (infiltration excess), simple-TOPMODEL (Niu et al., 2005) (saturation excess), and the runoff coefficient method (Feng et al., 2019) (conceptual). Each approach is coupled within one routing model (i.e., Hillslope River Routing model, HRR (Beighley et al., 2009)) to investigate the impacts of model structures and associate parameters on simulated streamflow. Compared to runoff generation process models, routing process models have less variants with most models using approximations of the Saint-Venant equations (Reed et al., 2004). Therefore, only one routing model is included in this study, however, this modeling framework is suitable to integrate different routing process models (e.g., diffusive wave and full dynamic solutions) and runoff schemes in future studies. This modeling framework is also coupled with a Bayesian model averaging (BMA) analysis to assess the performance of different model-forcing-parameter combinations and to provide actionable information (e.g., probability of estimated changes) for associated practices, such as water resource management and ecology conservation.

A case study is presented for Santa Barbara County, CA, a biodiverse region under a Mediterranean climate with a mix of highly developed and natural watersheds. To estimate future streamflow and associate uncertainties, the hydrologic models are forced with climate projections from 10 GCMs selected for their good performance in representing historical meteorological characteristics in the study region, under 2 emission scenarios (RCP 4.5 and RCP 8.5) (Feng et al., 2019). The main objectives of this study are to: (1) evaluate and compare the performance of hydrologic models with different approaches representing runoff generation process using a consistent modeling framework; (2) quantify the relative contributions of different sources (including hydrologic process models, parameterizations, GCM forcings and emission scenarios) to the total uncertainty in simulated streamflow; and (3) provide actionable information and suggestions for studies and practices associated with the hydrologic impacts of climate change in the study region.

2. Methods

2.1 Study region

The study region is located in coastal Santa Barbara County (SBC), California, where watersheds drain into the Santa Barbara Channel from just west of the Ventura River to just east

https://doi.org/10.5194/hess-2019-328
Preprint. Discussion started: 3 July 2019

of Point Conception (Fig. 1). The combined land area is roughly 750 km2 with 135 watersheds ranging from 0.1 to 123 km2. The local climate is Mediterranean, with an average annual precipitation of roughly 600 mm (Feng et al., 2019). Most of the annual precipitation occurs in fall/winter with 85% of rainfall occurring in the November-March period. Thus, it is characterized by the intense and flashy floods in winter time. More than 80% of annual discharge occurs in only a few number of large events during January-March and a large fraction of annual discharge happens within one day (Beighley et al., 2003). River channels are typically filled with sediment during dry season (April-October) and are scoured with the initiation of wet season floods (Scott and Williams, 1978;Keller and Capelli, 1992). River flow is the major source of sediment exported to the coastal sandy beaches in SBC. Therefore, the timing of seasonality and magnitudes of flood events are critical to both local community and coastal ecosystems.

2.1 Data

Daily precipitation and temperature with a spatial resolution of 0.0625° x 0.0625° (roughly 6 by 6 km) (Livneh et al., 2015), and daily streamflow from 4 USGS gauges for the period 1984-2013 are used to calibrate and validate the hydrologic model. The Global Soil Dataset for use in Earth system models (GSDE) is used to estimate saturated hydraulic conductivity and saturated moisture content. The 16-day composite albedo product (MCD43C3) with a spatial resolution of 0.05° x 0.05° and the monthly aerosol optical depth product (MOD08M3) with a spatial resolution of 1.0° x 1.0° both derived from NASA's Moderate Resolution Imaging Spectroradiometer (MODIS) are used to determine net radiation for evapotranspiration (PET) estimation.

For the historical (1986-2005) and future climate simulations (2081-2100), downscaled precipitation and temperature from ten climate models (please refer to Pierce et al. (2014) and Pierce et al. (2015) for model details) in Coupled Model Inter-Comparison Project, Phase 5, (CMIP5) (Taylor et al. 2012) for two emission scenarios RCP 4.5 and RCP 8.5 (Moss et al. 2010) are used. These 10 GCMs are selected because they have the best performance in representing historical climate dynamics at southwest U.S. and California state scales (Pierce et al., 2018).

2.2 Hydrologic modeling framework

2.2.1 Hydrologic model development

This modeling framework is developed on the basis of the Hillslope River Routing model (HRR) (Beighley et al., 2009). The watershed is delineated based on the Digital Elevation Model (DEM). The sub-basins are irregular-shape catchments defined by the flow accumulation area threshold. In this study, the threshold is 1 km^2, which means the sub-basins (model units) are in size of roughly 1 km^2. The hydrogeological model inputs, including surface roughness, saturated hydraulic conductivity, soil thickness, porosity, plane slope, channel slope and channel roughness, are averaged over each sub-basin. The geometry of each sub-basin (plane length and width) is calculated based on an “open-book” assumption, which assumes each sub-basin is a rectangular divided by the river channel into two identical parts like an open book. Please refer to Beighley et al. (2009) for more details. The precipitation and ET are extracted from the grid-based datasets for each sub-basin using an area-weighted average method. Then the water-balance model (i.e., runoff generation method) is applied to each model unit to simulate runoff generation processes. Here, three runoff generation methods: runoff coefficient (Feng et al., 2019), and the methods used in Variable Infiltration Capacity (VIC) (Wood et al., 1992;Liang et al., 1996) and simple-TOPMODEL model (Niu et al., 2005), are used to simulate the generation of surface and subsurface runoff excess. The routing methods within the HRR model (i.e., kinematic wave for surface and subsurface lateral routing and Muskingum-Cunge for channel routing) are used to simulate the transport of runoff excess. To clarify, we denote the three runoff generation algorithms: runoff coefficient, runoff generation method used in Variable Infiltration Capacity and runoff generation method used in simple-TOPMODEL as RCM, VIC and STP, respectively. The three hydrologic models which integrate each of these runoff generation methods with the routing method used in HRR model are referenced as RCM-HRR, VIC-HRR and STP-HRR, respectively. The differences between simulations from these three models are considered as the uncertainty resulting from hydrologic model formulation. The three runoff generation algorithms, and the surface, subsurface and channel routing are described below.

The RCM assumes water excess available for surface runoff (e_s) is proportional to precipitation rate (P). The proportion is represented by a coefficient value (e.g., 0 to 100%) and is dependent on land cover, soil and topographic characteristics. The coefficient value is smaller for dry and flat areas with permeable soils and vegetated surfaces, as compared to that for wet and steep areas with more impervious areas (e.g., roads, parking lots, roofs). In this work, a dual runoff-coefficient method is used, which assigns a larger runoff coefficient (C_2) to wet soils

https://doi.org/10.5194/hess-2019-328
Preprint. Discussion started: 3 July 2019

Hydrology and Earth System Sciences
Open Access
Discussions

(relative soil moisture at upper soil layer $\theta_U \geq$ threshold θ_t) and smaller runoff coefficient (C_1) to dry soils (relative soil moisture θ_U < threshold θ_t) (Eq. (1)). The water excess available for subsurface runoff (e_{ss}) is a function of saturated hydraulic conductivity (k_{sat}) and relative soil moisture in lower soil layer (θ_L) (Eq. (2)).

$$\begin{aligned} e_s &= C_1 \times P \quad for\ \theta_U < \theta_t \\ &= C_2 \times P \quad for\ \theta_U \geq \theta_t \end{aligned} \tag{1}$$

$$e_{ss} = K_{sat\_all} k_{sat} \times (\frac{\theta_L}{n})^b \tag{2}$$

where e_s and e_{ss} are water excess available for surface and subsurface runoff, respectively, (m d^{-1}); P is precipitation rate (m d^{-1}); C_1 is dry runoff coefficient; C_2 is wet runoff coefficient; θ_U and θ_L are relative soil moisture at upper and lower soil layer, respectively; θ_t is relative soil moisture threshold differentiating dry and wet soil conditions; k_{sat} is saturated hydraulic conductivity (m d^{-1}); K_{sat_all} is a scaler; b is Clapp-Hornberger parameter and n is soil porosity. C_1, C_2, θ_t and K_{sat_all} are parameters needing calibration.

In the VIC algorithm, surface runoff is generated as infiltration excess where the infiltration rate is characterized by the variable infiltration curve (Wood et al., 1992). In this work, the framework of modified 2-layer VIC model (VIC-2L) (Liang et al., 1996) is used. The water excess available for surface runoff is calculated as shown in Eq. (3)-(4). The water excess available for subsurface runoff is a function of soil moisture in lower soil layer (Eq. (5)), which is a linear function of soil moisture when the soil is relatively dry and quadratic when the soil is close to saturation:

$$e_s = P - z(\theta_s - \theta_U)/\Delta t - z\theta_s \left(max \left| 0, \left[1 - \frac{i_o + P\Delta t}{i_m} \right] \right| \right)^{1+b_i} /\Delta t \tag{3}$$

$$i_o = i_m \left[1 - (1 - A)^{1/b_i} \right] \tag{4}$$

$$e_{ss} = \frac{D_S D_M}{W_S \theta_S} \theta_L + \left(D_M - \frac{D_S D_M}{W_S} \right) \left(\frac{max|0, \theta_L - W_S \theta_S|}{\theta_S - W_S \theta_S} \right)^2 \tag{5}$$

where z is soil depth in upper layers (m); θ_s is relative soil moisture at saturation; i_m is maximum infiltration capacity (m); i_0 is infiltration capacity (m); b_i is infiltration curve parameter; A is the fraction of saturation; D_M is maximum base flow (m d^{-1}); D_S is the fraction of D_M at which the non-

https://doi.org/10.5194/hess-2019-328
Preprint. Discussion started: 3 July 2019

linear base flow begins; W_S is the fraction of saturation at which the non-linear base flow occurs; Δt is time step (d). b_i, D_M, D_S and W_S are parameters which need calibration.

In STP algorithm, the surface runoff is generated as saturation excess overland flow (Eq. (6)). The saturation fraction of the catchment f_{sat} is determined as a function of topographic index (Eq. (7)-(8)).

$$e_s = f_{sat} * P \tag{6}$$

$$f_{sat} = f_{max} * \exp(-0.5\, z_\nabla\, f_{over}) \tag{7}$$

where f_{sat} is the fraction of saturated area; f_{over} is a decay factor for surface runoff water excess (m^{-1}); z_∇ is groundwater table depth (m); f_{max} is the maximum saturated fraction and is defined as the percent of grid cells in each sub-basin with a topographic index (τ) that is ≥ the mean τ determined by averaging all grid cell τ values:

$$\tau = \ln\left(\frac{a}{tan(\beta)}\right) \tag{8}$$

where a is the specific catchment area (i.e.,upslope area per unit contour length) and β is the pixel slope. The specific catchment area a and slope β are calculated for grid cell using the gridded elevation data and the TauDEM tools (Tarboton, 2003).

The water excess available for subsurface runoff is a function of maximum base flow rate and groundwater table depth:

$$e_{ss} = Q_m * \exp(-f_{drain} * z_\nabla) \tag{9}$$

where f_{drain} is a decay factor for subsurface runoff water excess (m^{-1}), and Q_m is the maximum baseflow rate (m d^{-1}). Water excess for both surface and subsurface runoff are dependent of the groundwater table depth z_∇. Here, the water table depth z_∇ is determined by applying the method used in (Niu et al., 2005), which assumes the water head at depth z is in equilibrium with that at ground water depth z_∇ (Eq. (10)-(13)).

$$\varphi(z) - z = \varphi_{sat} - z_\nabla \tag{10}$$

https://doi.org/10.5194/hess-2019-328
Preprint. Discussion started: 3 July 2019

where $\varphi(z)$ and φ_{sat} are the metric potentials at depth z and at groundwater table depth z_∇ (m). The soil at the groundwater table depth is assumed to be saturated. Based on Clapp-Hornberger relationship (Clapp and Hornberger, 1978), $\varphi(z)$ can be expresses as:

$$\varphi(z) = \varphi_{sat}(\frac{\theta(z)}{\theta_{sat}})^{-b} \quad (11)$$

where θ(z) and θ_{sat} are soil moisture content at depth z and groundwater table depth z_∇, respectively, b is a Clapp-Hornberger parameter. By substituting Eq. (10) with Eq. (11), the soil matric profile at depth z can be expressed as:

$$\theta(z) = \theta_{sat}(\frac{\varphi_{sat} - (z_\nabla - z)}{\varphi_{sat}})^{-1/b} \quad (12)$$

Then, the groundwater table depth (z_∇) can be determined by solving Eq.13 iteratively.

$$D_\theta = \int_0^{z_\nabla} (\theta_{sat} - \theta(z))dz \quad (13)$$

where D_θ is the soil moisture deficit, which can be calculated in Eq.14:

$$D_\theta = \sum_{i=1}^{m} (\theta_{sat} - \theta_i)\nabla z_i \quad (14)$$

where θ_i is the soil moisture content at the ith soil layer; ∇z_i is the soil thickness of ith soil layer, m is the number of soil layer, m=2 in this study. In STP algorithm, f_{over}, f_{drain}, Q_m and φ_{sat} are parameters to be calibrated.

The water movement between soil layers in the soil matrix is similar to that in the modified VIC-2L model (Liang et al., 1996). The soil is divided into 2 layers: upper layer (0.6 m) and lower layer (2.6 m). The soil thickness data is determined based on a previous study (Feng et al., 2019). After the surface runoff is determined using the methods mentioned previously, the infiltrated water is added to the upper soil layer, and the soil moisture is updated. If the upper soil is oversaturated, the excess water is returned to surface. The interaction between upper and lower soil layers is determined using the Clapper-Hornberger equation (Eq. (15)-(16)). Subsurface runoff is generated from the bottom of the lower soil layer. The water flux from the upper layer does not contribute to runoff and is only lost to evapotranspiration and/or drainage to the lower soil layer. A conceptual illustration of the runoff generation process for each method and the water movement in soil matrix can be found in *Supporting Information Fig. S1*.

$$K = k_{sat} \times (\frac{\theta_U}{n})^c \tag{15}$$

$$D = k_{sat} \times (\frac{\theta_L}{n})^c \tag{16}$$

where K is the water flux from the upper soil layer to the lower soil layer (m d^{-1}); and D is the water flux transported from the lower soil layer to the upper soil layer due to diffusion (m d^{-1}).

After water excess for surface and subsurface runoff is determined, the kinematic wave approach is used to simulate the transport of runoff from the planes (surface and subsurface), and the Muskingum Cunge method is used for channel routing following the below conservation equations (Beighley et al., 2009):

Plane Routing:

$$\frac{\partial y_s}{dt} + \frac{\partial q_s}{dx_p} = e_s \tag{17}$$

$$\frac{\partial y_{ss}}{dt} + \frac{\partial q_{ss}}{dx_p} = e_{ss} \tag{18}$$

Channel Routing:

$$\frac{\partial A_c}{dt} + \frac{\partial Q_c}{dx_c} = q_s + q_{ss} \tag{19}$$

where y_s and y_{ss} are water depth (or thickness) of surface and subsurface runoff, respectively (m); q_s and q_{ss} are surface and subsurface runoff flow rates per unit width of plane (m^2 s^{-1}); dx_p is the distance step along the plane (m); A_C is the cross section area of flow in the channel (m^2); Q_c is the flow rate in channel (m^3 s^{-1}); dx_c is the distance step along the channel (m); and *dt* is the time step (s).

2.3.2 Model calibration

https://doi.org/10.5194/hess-2019-328
Preprint. Discussion started: 3 July 2019

After the models are setup, a state-of-the-art optimization algorithm, Borg Multiobjective Evolutionary Algorithm (Borg MOEA) (Hadka and Reed, 2013), is adopted to optimize the model parameters (Table 1). The parameters of the three models are calibrated separately. For each model, there are 4 parameters calibrated for runoff generation processes and 2 parameters calibrated for routing processes. K_{s_all} and K_{ss_all} are conceptual parameters which account for spatial heterogeneity at the model unit scale and uncertainties in the hydro-geologic inputs associated with the plane routing processes (e.g., surface roughness and saturated hydraulic conductivity). They can be different for different model structures even for the same study region. Therefore, they are calibrated for each model separately. The Nash–Sutcliffe model efficiency coefficient (NSE) (Eq. (20)) is used to assess model performance, as it accounts for model performance in terms of both timing and magnitudes of peak flow and base flow that are particularly important in this study. The optimal parameter set is determined after the improvement of error is minimized (here it is defined as ΔNSE<0.005). To quantify the uncertainties from model parameters, 3 optimal parameter sets with similar performance are selected for each model. The selected parameter sets are then used for simulation with different climate forcings.

$$\mathrm{NSE} = 1 - \frac{\sum_{t=1}^{T}(Q_s^t - Q_o^t)^2}{\sum_{t=1}^{T}(Q_o^t - \overline{Q_o})^2} \tag{20}$$

where Q_s^t and Q_o^t are simulated and observed discharge at time t, respectively, ($m^3\,s^{-1}$); and $\overline{Q_o}$ is the mean discharge during the study period of length T, ($m^3\,s^{-1}$).

2.3 Uncertainty Analysis

The uncertainty is quantified by running each of the 9 hydrologic model-parameter sets (i.e., 3 hydrologic models and 3 parameter sets, 3x3 = 9) with each of the 20 forcing sets (i.e., 10 GCMs and 2 emission scenarios, 10x2=20) for a total of 180 simulations.

To evaluate the uncertainty sources and their relative significance in simulated discharges for the future period, the analysis of variance (ANOVA) (Vetter et al., 2015) is used. The contribution of each uncertainty source for a particular variable (e.g., annual mean discharge, annual peak discharge or 100-yr flood discharge) is defined as the fraction of its variance to the total variance. The total variance is quantified as the total sum of squares (SS_{total}) of differences between the simulations and the mean of all simulations (Eq. (21)):

Hydrology and Earth System Sciences
Open Access
Discussions

$$SS_{Total} = \sum_{i=1}^{N_{Hyd}} \sum_{j=1}^{N_{para}} \sum_{k=1}^{N_{GCM}} \sum_{l=1}^{N_{RCP}} (q_{ijkl} - q_{oooo})^2 \tag{21}$$

where q_{ijkl} is the simulated value of a particular variable by ith hydrologic model with jth parameter set, forced by kth GCM projection under lth RCP scenario; q_{oooo} is the overall average of the simulated variable. Next, the SS_{Total} can be divided into 15 parts representing the 4 main effects (or first-order effects), 6 second-order, 4 third-order and 1 fourth-order interaction effects. For clarity, the third and fourth orders of interaction effects are combined and represented as $SS_{3.4}$ in Eq. (22).

$$\begin{aligned} SS_{Total} = {} & SS_{Hyd} + SS_{para} + SS_{GCM} + SS_{RCP} + SS_{Hyd.para} + SS_{Hyd.GCM} \\ & + SS_{Hyd.RCP} + SS_{para.GCM} + SS_{para.RCP} + SS_{GCM.RCP} \\ & + SS_{3.4} \end{aligned} \tag{22}$$

where $SS_{Hyd}, SS_{para}, SS_{GCM}$ *and* SS_{RCP} are the main effects (i.e., uncertainties or variance) from hydrologic models, parameterization, GCMs and RCPs, respectively; $SS_{Hyd.para}$, $SS_{Hyd.GCM}$, $SS_{Hyd.RCP}$, $SS_{para.GCM}$, $SS_{para.RCP}$ and $SS_{GCM.RCP}$ are uncertainties from interactions between the hydrologic models and parameterization, hydrologic models and GCMs, hydrologic models and RCPs, parameterization and GCMs, parametrization and RCPs, and GCMs and RCPs, respectively. The calculation of the effect of each order is illustrated in Eq. (23)-(25).

$$SS_{Hyd} = N_{para} N_{GCM} N_{RCP} \sum_{i=1}^{N_{Hyd}} (q_{iooo} - q_{oooo})^2 \tag{23}$$

$$SS_{Hyd.para} = N_{GCM} N_{RCP} \sum_{j=1}^{N_{para}} \sum_{i=1}^{N_{Hyd}} (q_{ijoo} - q_{iooo} - q_{ojoo} + q_{oooo})^2 \tag{24}$$

$$\begin{aligned} SS_{3.4} = {} & SS_{Total} - (SS_{Hyd} + SS_{para} + SS_{GCM} + SS_{RCP} + SS_{Hyd.para} \\ & + SS_{Hyd.GCM} + SS_{Hyd.RCP} + SS_{para.GCM} + SS_{para.RCP} \\ & + SS_{GCM.RCP}) \end{aligned} \tag{25}$$

https://doi.org/10.5194/hess-2019-328
Preprint. Discussion started: 3 July 2019

where q_{iooo} is the average of all simulations from the ith hydrologic model with all combinations of parameter sets, GCMs and RCPs; q_{ojoo} *is* the average of all simulations from the jth parameter set with all combinations of hydrologic models, GCMs and RCPs; q_{ijoo} is the average of all simulations from the ith hydrologic model and jth parameter set with all combinations of GCMs and RCPs. Other terms in Eq. (22) can be calculated similarly using Eq. (23)-(24).

To avoid bias from the difference in sample sizes of uncertainty sources (i.e., 3 hydrologic models, 3 parameter sets, 10 GCMs and 2 RCPs), a subsampling step is performed by following Vetter et al. (2015). In the subsampling step, 2 samples (the minimum number of uncertainty source, here it is RCPs) from each source are randomly selected, that is, 2 hydrologic models, 2 parameter sets, 2 GCMs and 2 RCPs, which means N_{Hyd}, N_{para}, N_{GCM} and N_{RCP} in Eq. (21), (23)-(24) are all equal to 2. This produces $C_3^2 \times C_3^2 \times C_{10}^2 \times C_2^2$=405 subsamples. For each subsample, the fractional sum of squares is calculated for each effect using Eq. (23)-(25), and then the average of variance fractions of each source is used as the uncertainty contribution from that source using Eq. (26):

$$\delta_e = \frac{1}{405} \sum_{m=1}^{405} \frac{SS_e(m)}{SS_{Total}(m)} \tag{26}$$

where δ_e is the average fractional effect of term e (i.e, each of 11 terms in Eq. (22)); $SS_e(m)$ is the sum of variance of effect e in the mth subsample, and the $SS_{Total}(m)$ is the total variance in the mth subsample. So in this study, there are 11 δ_e values in total, representing the uncertainty contributions of 11 terms in Eq. (22), with a sum of 1.0.

2.5 Probability of estimated changes

In addition to the quantification of uncertainties and associated contributions from different sources, an evaluation on the probability of uncertain changes in discharge can be useful to provide actionable information for the stakeholders such as water resource mangagers. In this study, the Bayesian model averaging (BMA) (Duan et al., 2007) is used to evaluate the model performance in reproducing historical hydrologic conditions and then assign weights to each of them based on their performance. A model with better performance will be assigned a higher weight, which assumes it has a higher probability to be the truth. Note, there is no RCPs for historical period, so only combinations of hydrologic models, parameter sets and GCMs (3x3x10=90) are evaluated.

https://doi.org/10.5194/hess-2019-328
Preprint. Discussion started: 3 July 2019

Hydrology and Earth System Sciences
Discussions

Here the models' performance in representing annual mean discharge (Q_m) and annual maximum daily discharge (Q_p) is evaluated. The details of this procedure can be found in Chapter 6 in Feng (2018).

After the weights of model ensemble are obtained using the BMA method, the statistics of posterior probability distribution (here it is assumed to be normal distribution) of estimated changes in Qm, Qp and Q_{100} in the future (2081-2100) relative to historical period 1986-2005 are calculated using Eq. (27)-(32).

For Q_m, the statistics are:

$$\mu_m = \sum_{k=1}^{K} w_{k,m} \times c_{k,m} \tag{27}$$

$$\sigma_m{}^2 = \sum_{k=1}^{K} w_{k,m} \times (c_{k,m} - \mu_m)^2 \tag{28}$$

where μ_m and σ_m are the mean and standard deviation of posterior distribution of relative changes in Q_m; $w_{k,m}$ is the weight of model k in terms of Q_m; $c_{k,m}$ is the relative change in Q_m predicted by model k; K is the total number of models, and here it is 90.

For Qp, the statistics are:

$$\mu_p = \sum_{k=1}^{K} w_{k,p} \times c_{k,p} \tag{29}$$

$$\sigma_p{}^2 = \sum_{k=1}^{K} w_{k,p} \times (c_{k,p} - \mu_p)^2 \tag{30}$$

where μ_p and σ_p are the mean and standard deviation of posterior distribution of relative changes in Q_p; $w_{k,p}$ is the weight of model k in terms of Q_p; $c_{k,p}$ is the relative change in Q_p predicted by model k.

For Q_{100}, the statistics are:

$$\mu_{100} = \sum_{k=1}^{K} w_{k,p} \times c_{k,100} \tag{31}$$

$$\sigma_{100}{}^{2} = \sum_{k=1}^{K} w_{k,p} \times (c_{k,100} - \mu_{100})^{2} \tag{32}$$

where μ_{100} and σ_{100} are the mean and standard deviation of posterior distribution of relative changes in Q_{100}; $w_{k,p}$ is the weight of model k for Q_p; $c_{k,100}$ is the relative change in Q_{100} predicted by model k. Here, the weights for Q_p are used because Q_{100} is estimated based on the statistics of Q_p series, so it is reasonable to assume that the model having a better ability in reproducing the annual peak discharge should also have a better ability in reproducing the Q_{100}.

3 Results and Discussion

3.1 Hydrologic model performance

The three hydrologic models perform well in representing streamflow dynamics in the study region. The NSE varies within 0.57-0.61 and 0.53-0.62 for calibration and validation periods, respectively, in Mission Creek (gauge NO. 11119750) (Fig. 2). At other calibrated watersheds, the models perform similarly well with NSE varying between 0.45-0.60 for calibration period and 0.42-0.62 for validation period (Fig. S2-S4). Simulated streamflow from the three models matches the in-situ measurements in both magnitudes and timing of hydrographs at event scales (Fig. 2b). At annual scale, simulated annual peak flows are comparable to the observations in most years. However, in some years with extremely high events, for example in 1995 January, 1998 February and 2005 January (highlighted in Fig. 2c), the simulated peaks are much lower than the gauge records. This disparity can be attributed to the input bias (e.g., precipitation or streamflow measurements). This is identified using an 'extreme scenario' simulation, which assumes 100% precipitation is transformed to surface runoff (i.e., without any loss due to, for example, infiltration or evapotranspiration) and transported immediately to river channels and represents the maximum streamflow considering groundwater is minimal in the study region(Beighley et al., 2003). Even for this extreme scenario, the simulated peaks were still lower (events highlighted in red in Fig. 2c) or slightly higher (event highlighted in blue in Fig. 2c) than the gauge observations. This is likely because that model forcings are bias low for these events. One possible source of this bias can be the grid-based precipitation dataset which averages the precipitation rates over the grid masking spatial heterogeneity and thus reducing precipitation rates at some locations. The uncertainties in gauge measurements can also be a bias source. For example, in typical conditions the uncertainty in streamflow measurements ranges between 6%-19% in small watersheds, but it can be higher during large storm events when accurate stage measurements are more difficult (Harmel et al., 2006). Beighley et al. (2003) also identified the overestimation of gauge records at Gauge 11119940 during the 1995 January event. As for mean annual discharge, all three models tend to overestimate for the study period, mainly due to the overestimation of subsurface flow during dry seasons (Fig. 2d). This highlights challenges of simulating hydrologic processes in semiarid regions under a Mediterranean climate.

Among the three hydrologic models, STP-HRR has the best overall performance (i.e., highest average NSE), mainly due to its better ability for capturing flood peaks than the other 2 models (Fig. 2, S2-S4). The peak performance is likely a result of the STP-HRR representing the runoff generation process as an exponential relationship between soil moisture and runoff rates, which makes runoff generation more sensitive to soil moisture dynamics as compared to the other 2 models. This algorithm is well suited to represent the significant nonlinearity of hydrologic response to rainfall in the study region. RCM-HRR and VIC-HRR have similar overall performance (i.e., similar average NSE), however, they represent hydrologic dynamics differently. VIC-HRR tends to perform better in representing small peak flows than RCM-HRR while worse in simulating mean flow (or total discharge volume) (Fig. 2, S2-S4). This is because as the wet season proceeds, the lower soil layer is close to saturation (i.e., relative soil moisture is higher than the threshold W_s for VIC-HRR) which initiate the quadratic relationship between soil moisture and subsurface runoff in VIC-HRR. This quadratic response to soil moisture conditions can lead to much higher subsurface runoff (2-3 magnitudes higher than that of RCM-HRR), which contributes to the lower performance in reproducing the total volume of discharge. This also explains that VIC-HRR generates the highest subsurface runoff during the wet season (Fig. 3). In addition, VIC-HRR also generates the most surface runoff during wet season (Fig. 3). This is because when soil is almost saturated, surface runoff in VIC-HRR is almost a linear function of precipitation with a coefficient of 1 (much larger than RCM-HRR which is 0.2 (C_2) and STP-HRR which is around 0.5 depending on the watershed topography). The higher surface and subsurface runoff generated by VIC-HRR leads to the overestimation of mean annual flow (Fig. 2d). However, there are no in-

https://doi.org/10.5194/hess-2019-328
Preprint. Discussion started: 3 July 2019

situ measurement of surface and subsurface fluxes, and it is difficult to evaluate model performance for these quantities individually or as a ratio. In Fig. 3, the simulated surface and subsurface runoff from National Land Data Assimilation Systems VIC model (NLDAS-VIC) output is also shown for purpose of comparison. A similar pattern, i.e., a very high subsurface runoff, even higher than surface runoff, during wet season, can be found from NLDAS-VIC simulations. The surface runoff of NLDAS-VIC is lower than those generated by the models in this study, which is probably because of the difference in precipitation inputs. The NLDAS precipitation input is lower during wet season than that used in this study for the study region. In addition, the difference in spatial resolutions of precipitation (0.125° for NLDAS vs. 0.0625° for this study) can also contribute to the difference in simulated runoff.

These results may suggest that STP-HRR is more suitable than VIC-HRR in representing hydrologic processes in Mediterranean regions where 80% annual precipitation is concentrated in a short period (roughly 3 months). As the wet season proceeds, the soil is close to saturation conditions, under which the saturation excess overland flow is dominant. That explains why STP-HRR performs best in this study region. VIC-HRR is probably more suitable to the regions where precipitation events are sparsely distributed where soil is not easy saturated. Although RCM is an empirical method, it performs fairly well in this study, mainly because it captures the nonlinearity of hydrologic processes through a switch between dry and wet surface runoff coefficients (C_1 and C_2) based on the soil moisture conditions.

Three sets of parameters with the best performance (assessed by NSE) were selected for each model (Fig. 4). For most of parameters, the selected optimal values are very close, except C_1 and K_{s_all} in RCM-HRR, suggesting that most parameters are important factors controlling model performance. For some parameters whose optimal values are close to their range boundaries, for example, K_{ss_all}, W_s, φ_{sat} and Q_m, wider and physically acceptable ranges were tested and similar results were obtained, which suggests the ranges of these parameters defined in this study (Table 1) are reasonable.

3.2 Uncertainty analysis

For the 28 major watersheds in SBC, the projected changes in Q_m during 2081-2100 as compared to historical period 1986-2005, range from -80% to 150% (Fig. 5). The median changes for each of these major watersheds are slightly above 0%, varying between 1% and 10%. The

https://doi.org/10.5194/hess-2019-328
Preprint. Discussion started: 3 July 2019

major uncertainty sources are GCM and RCP, which account for about 50% of the total uncertainty. Among the first order factors (i.e., GCM, RCP, hydrologic model and parameterization), hydrologic model ranks third after GCM and RCP, accounting for about 10-20% of total uncertainty. In contrast, parameterization only introduces less than 1% of the total uncertainty. The remaining 30-40% uncertainty is from the second, third and fourth order interactions between the four major sources. The projected relative changes in Q_p and Q_{100} during 2081-2100 compared to 1986-2005 are similar in magnitudes, both varying from -90% to 240% (Fig. 6 and Fig. 7). The median changes in Q_p and Q_{100} for each watershed are higher than those of Q_m, ranging between 10-40%. For most of watersheds, GCM and RCP are the two major uncertainty contributors for Q_p and Q_{100}, accounting for 40-60% of total uncertainties. Hydrologic model contributes about 10-30% of total uncertainties in Q_p and Q_{100}. Compared to Q_m, Q_p and Q_{100} get more uncertainty from the hydrologic models, which is likely due to highly nonlinear rainfall-runoff behavior and larger differences between runoff generation methods in generating peak flows as compared to average flow conditions.

Changes in Q_m, Q_p and Q_{100} are higher under RCP 8.5, but the uncertainties are also higher (Fig. 8), which suggests the uncertainties from RCPs are mainly introduced by RCP 8.5. In Mission Creek watershed (USGS gauge No. 11119750), the probability of increase in Qm under RCP 4.5 is only 51%. However, this probability increases to 64% under RCP 8.5. For the less frequent events (Q_p and Q_{100}), the probabilities of positive changes are higher: 78% and 85% for Q_p and Q_{100}, respectively, under RCP 8.5. This implies that if RCP 8.5 happens in the future, the extreme events will probably get intensified.

Compared to previous studies (e.g., Vetter et al. (2015), Schewe et al. (2014), Hagemann et al. (2013);(Troin et al., 2018), and Asadieh and Krakauer (2017)), this work identifies relatively lower uncertainty contributions from hydrologic models. This is mainly because in this study the models use the same model configuration including the model unit definition (irregular catchments) and the hillslope routing scheme ("open-book" assumption), which reduces the difference between hydrologic models. Here, a common calibration approach is also used to eliminate user/method bias which is common in studies that consider more than one hydrologic model. In contrast, the hydrologic models used in previous studies are the individual models which use their own model configurations. For example, the VIC model (here VIC refers to the original VIC models, and is different from the model used in this study; to clarify, in following text, VIC

https://doi.org/10.5194/hess-2019-328
Preprint. Discussion started: 3 July 2019

refers to the original VIC model while VIC-HRR refers to the model used in this study) uses the grid-based model units ignoring the spatial arrangement and has its own routing scheme which adopts the synthetic unit hydrograph concept. These differences between models probably resulted in the larger uncertainties in the simulation from hydrologic models in previous studies.

Different from previous studies, the hydrologic model uncertainty in this study only comes from the runoff generation algorithms. This can provide useful information for selecting hydrologic models for climate change impact analysis. The results in this study imply that selecting an appropriate runoff generation algorithm suitable to the regions of interest and the study targets (e.g., total volume or extremes) can reduce uncertainties by 10-30%, especially for the extreme quantities (e.g., 100-yr flood discharge). Compared to the runoff generation algorithms, model parameterization plays a negligible role (less than 1%) in the total streamflow uncertainty. This suggests that the parameter equifinality (or non-uniqueness) is less of a concern when quantifying climate change impacts on hydrologic fluxes using an ensemble of GCM forcings. In this study, only one routing scheme is investigated. Although there are fewer variants of routing algorithms as compared to runoff generation methods, the choice of different routing methods can still make a difference in the total uncertainties in streamflow simulation, especially when the model configurations are different, for example, the routing schemes in VIC model and HRR model. Therefore, further study integrating different routing algorithms should be conducted to evaluate the uncertainties in simulated streamflow resulted from both process models (runoff generation model and routing model), which can be useful to guide stakeholders to select appropriate hydrologic algorithms for climate change impacts analysis and develop actionable adaptation and mitigation strategies.

4 Conclusions

A modeling framework which integrates multiple runoff generation algorithms (VIC, STP and RCM) with the Hillslope River Routing model (HRR) is developed. Forced with an ensemble of GCM projections under different emission scenarios, this framework is able to quantify the climate change impacts on streamflow and evaluate the associated uncertainties from different sources (i.e., RCPs, GCMs, hydrologic process models and parameterization). The results in this study show that the median changes in mean annual discharge for the major watersheds in SBC are 1-10%, with an uncertainty of 230% (-80% to +150%); the median changes in annual peak

https://doi.org/10.5194/hess-2019-328
Preprint. Discussion started: 3 July 2019

discharge and 100-yr flood discharge are higher than those of mean annual discharge, varying between 10% and 40%, but with a higher uncertainty of 330% (-90% to +240%). For these uncertainties, GCM and RCP are the first two major contributors, accounting for more than 50% of total uncertainties at most watersheds in SBC, while hydrologic process models (i.e., runoff generation modules) contribute between 10% and 30% among watersheds with the remaining 20-40% of the uncertainty coming from the interactions between these individual sources. Hydrologic model parameters alone contribute less than 1% of the uncertainty, which suggests the parameter equifinality should not be a concern when analyzing climate change impacts using ensembles of climate models projections. The results based on the BMA analysis indicate that there is a high probability (up to 85%) that streamflow, especially the extreme quantities like Q_{100} under RCP 8.5, will increase in SBC.

Unique to this framework, the uncertainties from different hydrologic model components (e.g., runoff generation process) and associated model parameterizations can be identified and quantified. In this study, only one routing scheme is integrated, however, this framework is capable of incorporating multiple routing methods to quantify their contributions to the uncertainties in simulated hydrologic variables. These information can help stakeholders with different focuses (e.g., water resources, risk controls or ecosystem conservation) customize and optimize their selections of hydrologic models and make actionable adaptation decisions under the changing climate.

Code availability

The source code supporting this work is available on Github: https://github.com/dongmeifeng-2019/HydroUncertainty

Author contribution

D. Feng and E. Beighley designed the experiments and D. Feng developed the model code and performed the simulations. D. Feng and E. Beighley prepared the manuscript.

Competing interests

The authors declare that they have no conflict of interest.

https://doi.org/10.5194/hess-2019-328
Preprint. Discussion started: 3 July 2019

Hydrology and Earth System Sciences
Discussions

Acknowledgments

This research was supported by the Santa Barbara Area Coastal Ecosystem Vulnerability Assessment (SBA CEVA) with funding from the NOAA Climate Program Office Coastal and Ocean Climate Applications (COCA) and Sea Grant Community Climate Adaptation Initiative (CCAI), and the National Science Foundation's Long-Term Ecological Research (LTER) program (Santa Barbara Coastal LTER - OCE9982105, OCE-0620276 and OCE-123277). The authors thank Dr. David Hadka at Pennsylvania State University and Chinedum Eluwa at University of Massachusetts, Amherst, for their help with setting up the Borg MOEA.

https://doi.org/10.5194/hess-2019-328
Preprint. Discussion started: 3 July 2019

Hydrology and Earth System Sciences
Open Access
Discussions

References:

Asadieh, B., and Krakauer, N. Y.: Global change in streamflow extremes under climate change over the 21st century, Hydrology and Earth System Sciences, 21, 5863, 2017.

Barnett, T. P., Adam, J. C., and Lettenmaier, D. P.: Potential impacts of a warming climate on water availability in snow-dominated regions, Nature, 438, 303-309, 2005.

Beighley, E., Eggert, K. G., Dunne, T., He, Y., Gummadi, V., and Verdin, K. L.: Simulating hydrologic and hydraulic processes throughout the Amazon River Basin, Hydrological Processes, 23, 1221-1235, 10.1002/hyp.7252, 2009.

Beighley, R. E., Melack, J. M., and Dunne, T.: Impacts of California's climatic regimes and coastal land use change on streamflow characteristics, JAWRA Journal of the American Water Resources Association, 39, 1419-1433, 10.1111/j.1752-1688.2003.tb04428.x, 2003.

Beven, K. J., and Cloke, H. L.: Comment on "Hyperresolution global land surface modeling: Meeting a grand challenge for monitoring Earth's terrestrial water" by Eric F. Wood et al, Water Resources Research, 48, 2012.

Cai, W., Borlace, S., Lengaigne, M., van Rensch, P., Collins, M., Vecchi, G., Timmermann, A., Santoso, A., McPhaden, M. J., Wu, L., England, M. H., Wang, G., Guilyardi, E., and Jin, F.-F.: Increasing frequency of extreme El Nino events due to greenhouse warming, Nature Clim. Change, 4, 111-116, 10.1038/nclimate2100, 2014.

Clapp, R. B., and Hornberger, G. M.: Empirical equations for some soil hydraulic properties, Water Resources Research, 14, 601-604, 10.1029/WR014i004p00601, 1978.

Dai, A.: The influence of the inter-decadal Pacific oscillation on US precipitation during 1923–2010, Climate dynamics, 41, 633-646, 2013.

Dettinger, M.: Climate change, atmospheric rivers, and floods in California - a multimodel analysis of storm frequency and magnitude changes, Journal of the American Water Resources Association, 47, 514-523, 10.1111/j.1752-1688.2011.00546.x, 2011.

Duan, Q., Ajami, N. K., Gao, X., and Sorooshian, S.: Multi-model ensemble hydrologic prediction using Bayesian model averaging, Advances in Water Resources, 30, 1371-1386, https://doi.org/10.1016/j.advwatres.2006.11.014, 2007.

Eisner, S., Flörke, M., Chamorro, A., Daggupati, P., Donnelly, C., Huang, J., Hundecha, Y., Koch, H., Kalugin, A., Krylenko, I., Mishra, V., Piniewski, M., Samaniego, L., Seidou, O., Wallner, M., and Krysanova, V.: An ensemble analysis of climate change impacts on streamflow seasonality across 11 large river basins, Climatic Change, 141, 401-417, 10.1007/s10584-016-1844-5, 2017.

Feng, D., Beighley, E., Hughes, R., and Kimbro, D.: Spatial and temporal variations in eastern U.S. Hydrology: Responses to global climate variability, JAWRA Journal of the American Water

Resources Association, 52, 1089-1108, 10.1111/1752-1688.12445, 2016.

Feng, D.: Characterizing Changes in Hydrologic Fluxes and Uncertainties for Current and Future Climate Conditions. , PhD, Civil and Environmental Engineering, Northeastern University, Boston, MA, 2018.

Feng, D., Beighley, E., Raoufi, R., Melack, J., Zhao, Y., Iacobellis, S., and Cayan, D.: Propagation of future climate conditions into hydrologic response from coastal southern California watersheds, Climatic Change, 153, 199-218, 10.1007/s10584-019-02371-3, 2019.

Hadka, D., and Reed, P.: Borg: An auto-adaptive many-objective evolutionary computing framework, Evolutionary computation, 21, 231-259, 2013.

Hagemann, S., Chen, C., Clark, D. B., Folwell, S., Gosling, S. N., Haddeland, I., Hanasaki, N., Heinke, J., Ludwig, F., Voss, F., and Wiltshire, A. J.: Climate change impact on available water resources obtained using multiple global climate and hydrology models, Earth Syst. Dynam., 4, 10.5194/esd-4-129-2013, 2013.

Harmel, R. D., Cooper, R. J., Slade, R. M., Haney, R. L., and Arnold, J. G.: Cumulative uncertainty in measured streamflow and water quality data for small watersheds, Transactions of the ASABE, 49, 689-701, 2006.

Horton, R. E.: The Rôle of infiltration in the hydrologic cycle, Eos, Transactions American Geophysical Union, 14, 446-460, 10.1029/TR014i001p00446, 1933.

Kay, A. L., Davies, H. N., Bell, V. A., and Jones, R. G.: Comparison of uncertainty sources for climate change impacts: flood frequency in England, Climatic Change, 92, 41-63, 10.1007/s10584-008-9471-4, 2009.

Keller, E. A., and Capelli, M. H.: VENTURA RIVER FLOOD OF FEBRUARY 1992: A LESSON IGNORED?1, JAWRA Journal of the American Water Resources Association, 28, 813-832, 10.1111/j.1752-1688.1992.tb03184.x, 1992.

Liang, X., Wood, E. F., and Lettenmaier, D. P.: Surface soil moisture parameterization of the VIC-2L model: Evaluation and modification, Global and Planetary Change, 13, 195-206, https://doi.org/10.1016/0921-8181(95)00046-1, 1996.

Livneh, B., Bohn, T. J., Pierce, D. W., Munoz-Arriola, F., Nijssen, B., Vose, R., Cayan, D. R., and Brekke, L.: A spatially comprehensive, hydrometeorological data set for Mexico, the U.S., and Southern Canada 1950–2013, Scientific Data, 2, 150042, 10.1038/sdata.2015.42, 2015.

Milly, P. C. D., Dunne, K. A., and Vecchia, A. V.: Global pattern of trends in streamflow and water availability in a changing climate, Nature, 438, 347-350, 2005.

Niu, G. Y., Yang, Z. L., Dickinson, R. E., and Gulden, L. E.: A simple TOPMODEL-based runoff parameterization (SIMTOP) for use in global climate models, Journal of Geophysical Research:

https://doi.org/10.5194/hess-2019-328
Preprint. Discussion started: 3 July 2019

Atmospheres, 110, doi:10.1029/2005JD006111, 2005.

Pierce, D. W., Cayan, D. R., and Thrasher, B. L.: Statistical downscaling using localized constructed analogs (LOCA), Journal of Hydrometeorology, 15, 2558-2585, 2014.

Pierce, D. W., Cayan, D. R., Maurer, E. P., Abatzoglou, J. T., and Hegewisch, K. C.: Improved Bias Correction Techniques for Hydrological Simulations of Climate Change, Journal of Hydrometeorology, 16, 2421-2442, 10.1175/jhm-d-14-0236.1, 2015.

Pierce, D. W., Kalansky, J. F., and Cayan, D. R.: Climate, drought, and sea level rise scenarios for California's fourth climate change assessment. , California Energy Commission and California Natural Resources Agency, 2018.

Reed, S., Koren, V., Smith, M., Zhang, Z., Moreda, F., Seo, D.-J., and Dmip Participants, a.: Overall distributed model intercomparison project results, Journal of Hydrology, 298, 27-60, https://doi.org/10.1016/j.jhydrol.2004.03.031, 2004.

Schewe, J., Heinke, J., Gerten, D., Haddeland, I., Arnell, N. W., Clark, D. B., Dankers, R., Eisner, S., Fekete, B. M., Colón-González, F. J., Gosling, S. N., Kim, H., Liu, X., Masaki, Y., Portmann, F. T., Satoh, Y., Stacke, T., Tang, Q., Wada, Y., Wisser, D., Albrecht, T., Frieler, K., Piontek, F., Warszawski, L., and Kabat, P.: Multimodel assessment of water scarcity under climate change, Proceedings of the National Academy of Sciences, 111, 3245-3250, 10.1073/pnas.1222460110, 2014.

Scott, K. M., and Williams, R. P.: Erosion and sediment yields in the Transverse Ranges, southern California, 38 p., 1978.

Su, B., Huang, J., Zeng, X., Gao, C., and Jiang, T.: Impacts of climate change on streamflow in the upper Yangtze River basin, Climatic Change, 141, 533-546, 10.1007/s10584-016-1852-5, 2017.

Tao, H., Gemmer, M., Bai, Y., Su, B., and Mao, W.: Trends of streamflow in the Tarim River Basin during the past 50years: Human impact or climate change?, Journal of hydrology, 400, 1-9, 2011.

Tarboton, D. G.: Terrain Analysis Using Digital Elevation Models in Hydrology, 23rd ESRI International Users Conference, San Diego, California, July 7-11, 2003.

Troin, M., Arsenault, R., Martel, J.-L., and Brissette, F.: Uncertainty of Hydrological Model Components in Climate Change Studies over Two Nordic Quebec Catchments, Journal of Hydrometeorology, 19, 27-46, 10.1175/jhm-d-17-0002.1, 2018.

Valentina, K., Tobias, V., Stephanie, E., Shaochun, H., Ilias, P., Michael, S., Alexander, G., Rohini, K., Valentin, A., Berit, A., Alejandro, C., Ann van, G., Dipangkar, K., Anastasia, L., Vimal, M., Stefan, P., Julia, R., Ousmane, S., Xiaoyan, W., Michel, W., Xiaofan, Z., and Fred, F. H.: Intercomparison of regional-scale hydrological models and climate change impacts projected for 12 large river basins worldwide—a synthesis, Environmental Research Letters, 12, 105002, 2017.

https://doi.org/10.5194/hess-2019-328
Preprint. Discussion started: 3 July 2019

Vetter, T., Huang, S., Aich, V., Yang, T., Wang, X., Krysanova, V., and Hattermann, F.: Multi-model climate impact assessment and intercomparison for three large-scale river basins on three continents, Earth System Dynamics, 6, 17, 2015.

Vicky, E., E., W. D., Bin, G., A., L. D., and Martin, R. F.: Global Analysis of Climate Change Projection Effects on Atmospheric Rivers, Geophysical Research Letters, 45, 4299-4308, doi:10.1029/2017GL076968, 2018.

Wilby, R. L., and Harris, I.: A framework for assessing uncertainties in climate change impacts: Low-flow scenarios for the River Thames, UK, Water Resources Research, 42, doi:10.1029/2005WR004065, 2006.

Wood, E. F., Lettenmaier, D. P., and Zartarian, V. G.: A land-surface hydrology parameterization with subgrid variability for general circulation models, Journal of Geophysical Research: Atmospheres, 97, 2717-2728, 10.1029/91JD01786, 1992.

https://doi.org/10.5194/hess-2019-328
Preprint. Discussion started: 3 July 2019

Hydrology and Earth System Sciences
Discussions

Table 1: Calibrated parameters for all 3 models

Parameters	Description	Unit	Range	RCM -HRR	VIC-HRR	STP-HRR
K_{s_all}	coefficient to adjust surface roughness	-	1-20	✓	✓	✓
K_{ss_all}	coefficient to adjust horizontal hydraulic conductivity	-	10-200	✓	✓	✓
K_{sat_all}	coefficient to adjust vertical hydraulic conductivity	-	0.01-5.0	✓		
C_1	dry runoff coefficient	-	0-0.3	✓		
C_2	wet runoff coefficient	-	0.2-0.8	✓		
θ_t	soil moisture threshold separating dry and wet conditions	-	0.2-0.8	✓		
b_{in}	Infiltration curve shape parameter	-	0.005-0.5		✓	
D_m	maximum baseflow	$m \cdot d^{-1}$	0 -0.037		✓	
D_s	fraction of D_M where non-linear baseflow begins	-	0 -0.005		✓	
W_s	fraction of the maximum soil moisture where non-linear baseflow occurs	-	0.92-1.0		✓	
f_{over}	Surface runoff coefficient	m^{-1}	0.1-5			✓
f_{drain}	Subsurface runoff coefficient	m^{-1}	0.1-5			✓
Q_m	maximum baseflow	$m \cdot d^{-1}$	0.864-1728			✓
φ_{sat}	Saturated suction head in the soil	m	-3.05–0			✓

https://doi.org/10.5194/hess-2019-328
Preprint. Discussion started: 3 July 2019

Hydrology and Earth System Sciences
Discussions

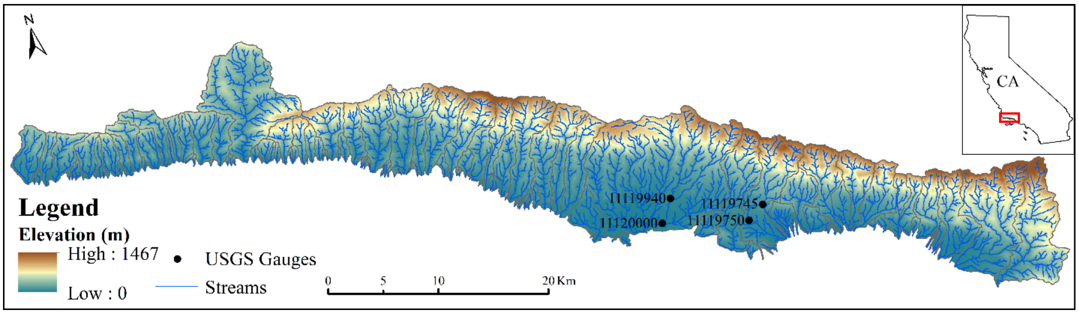

636 **Figure 1: Study region with USGS streamflow gauges. The inset figure indicates the**
637 **location of SBC within the state of California (CA).**

https://doi.org/10.5194/hess-2019-328
Preprint. Discussion started: 3 July 2019

Hydrology and Earth System Sciences
Discussions

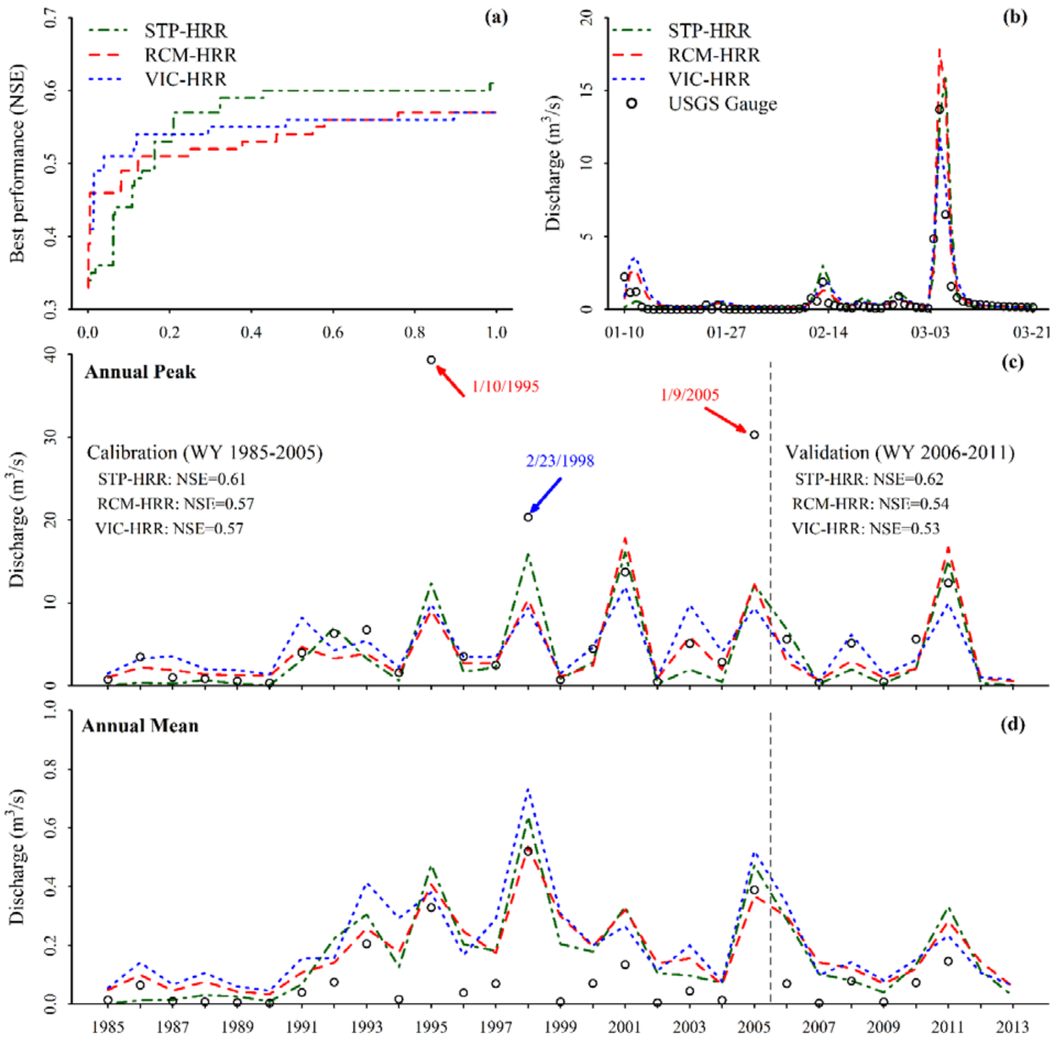

Figure 2 Model performance for calibration and validation periods: (a) model performance (assessed by NSE) during calibration process, x axis is the normalized calibration process; (b) hydrographs simulated by 3 calibrated models and measured by USGS gauge; in order to show the details of the hydrographs, they are zoomed in to the wet season in 2001; the model performance is similar in other years; (c) simulated annual peak flow during calibration (water year 1985-2005) and validation (water year 2006-2011) periods as compared with in situ observations; texts indicate model performance (i.e., NSE) in reproducing historical hydrographs for both periods; the points highlighted in red arrows indicate the events were not reproduced by models due to the input (e.g., precipitation or discharge observation) bias; the point highlighted in blue arrow is similar to those in red but at a lower probability; and (d) simulated and observed annual mean flow during calibration and validation periods. For clarity, only results for Mission Creek watershed (USGS gauge NO. 11119750) are shown here; results for other gauged watersheds are similar and can be found in the Supporting Information (Figure S1-S3).

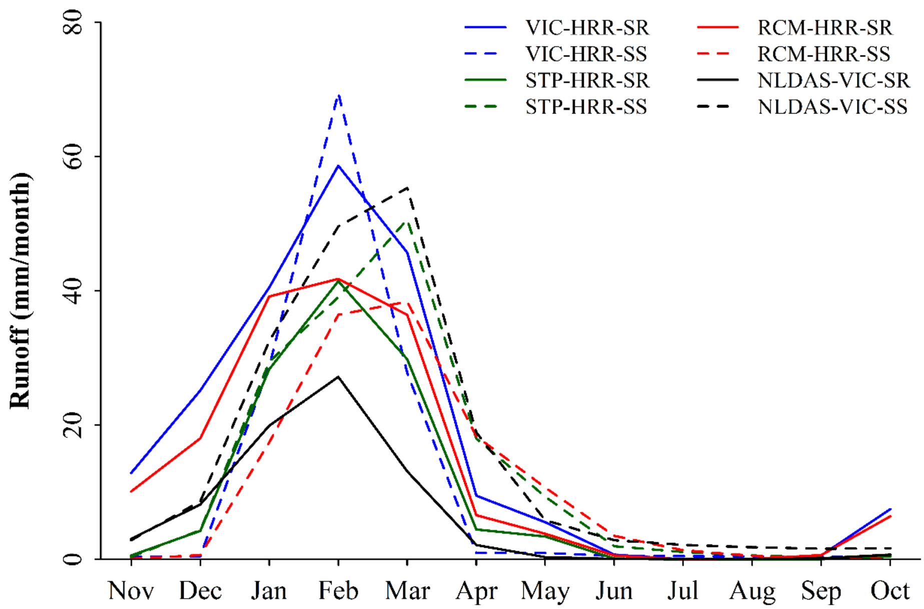

Figure 3: Simulated monthly surface and subsurface runoff from Mission Creek watershed (USGS gauge NO. 11119750) by three models for the calibration period (water year 1985-2005). Surface runoff is denoted by 'SR' and subsurface runoff is denoted by 'SS' in this figure. Monthly surface and subsurface runoff from National Land Data Assimilation Systems (NLDAS) VIC model simulation for the same period are shown here for comparison purpose.

https://doi.org/10.5194/hess-2019-328
Preprint. Discussion started: 3 July 2019

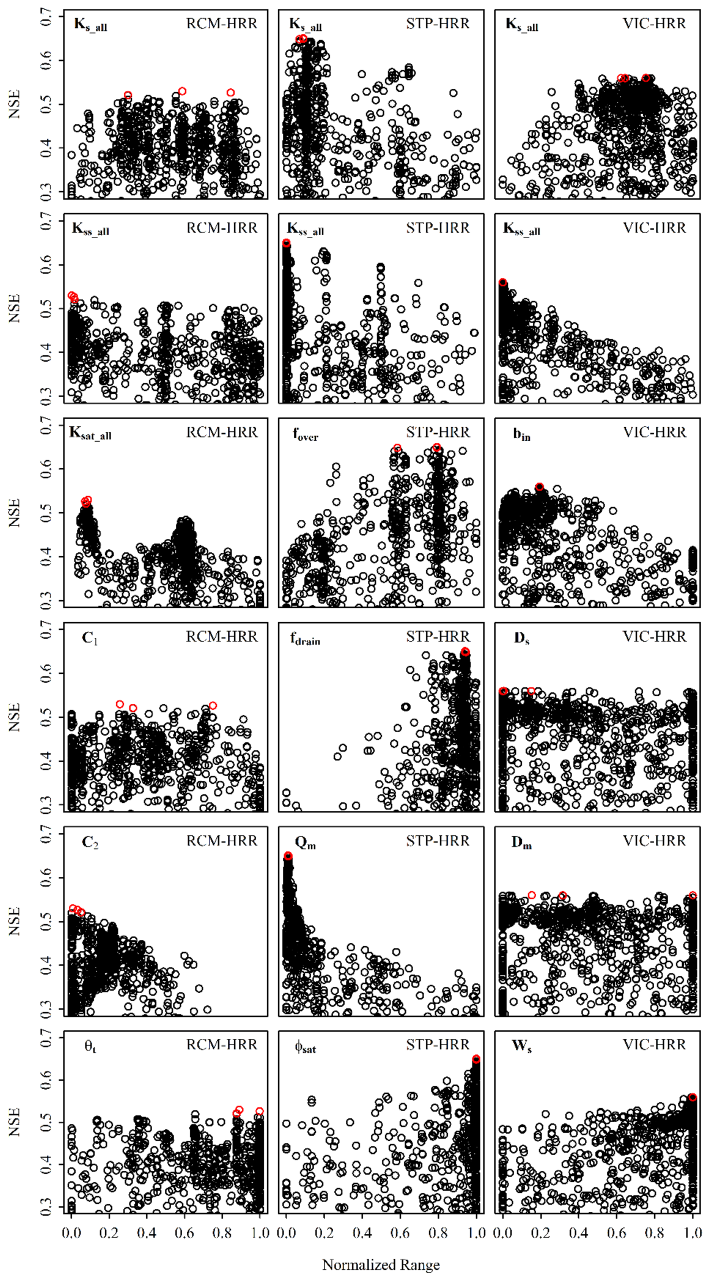

Figure 4. Parameters sampled during calibration process and their corresponding performance (assessed by NSE). The black circles are parameter samples within the predefined ranges (shown in Table 1) and the red circles indicate the optimal values used for further uncertainty analysis. The parameter values are normalized by their ranges, so the range of x axis in all plots is 0-1. The parameters were sampled throughout their whole ranges, however, for clarity, samples with NSE lower than 0.3 are not shown in this figure.

https://doi.org/10.5194/hess-2019-328
Preprint. Discussion started: 3 July 2019

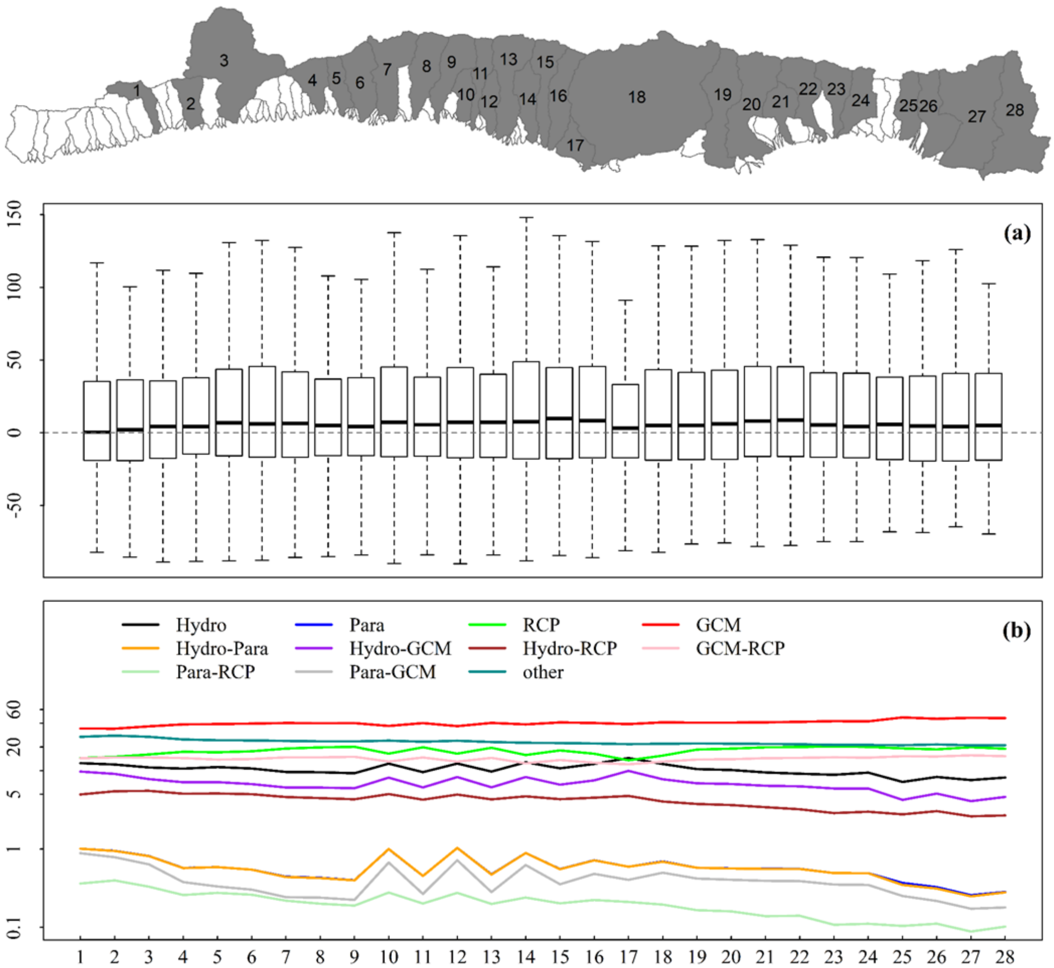

Figure 5. (a) Projected relative changes (%) in annual mean discharge (Q_m) in the major SBC watersheds (indicated by the grey watersheds in the map) during 2081-2100 as compared to historical period (1986-2005); each bar depicts relative changes in minimum, maximum, median, 1st and 3rd quartiles for the ensemble outputs; bars from left to right spatially corresponding to watersheds from west to east. For clarity, only watersheds with drainage areas larger than 7 km^2, which account for roughly 83% of the study area, are shown. (b) Relative sources (%) of the uncertainties in the projected changes at each of these watersheds; the category "other" is the uncertainty from the 3rd and 4th orders of interactions between the 4 major sources (i.e., GCMs, RCPs, Hydrologic models, denoted by "Hydro" and parameters denoted by "Para")

https://doi.org/10.5194/hess-2019-328
Preprint. Discussion started: 3 July 2019

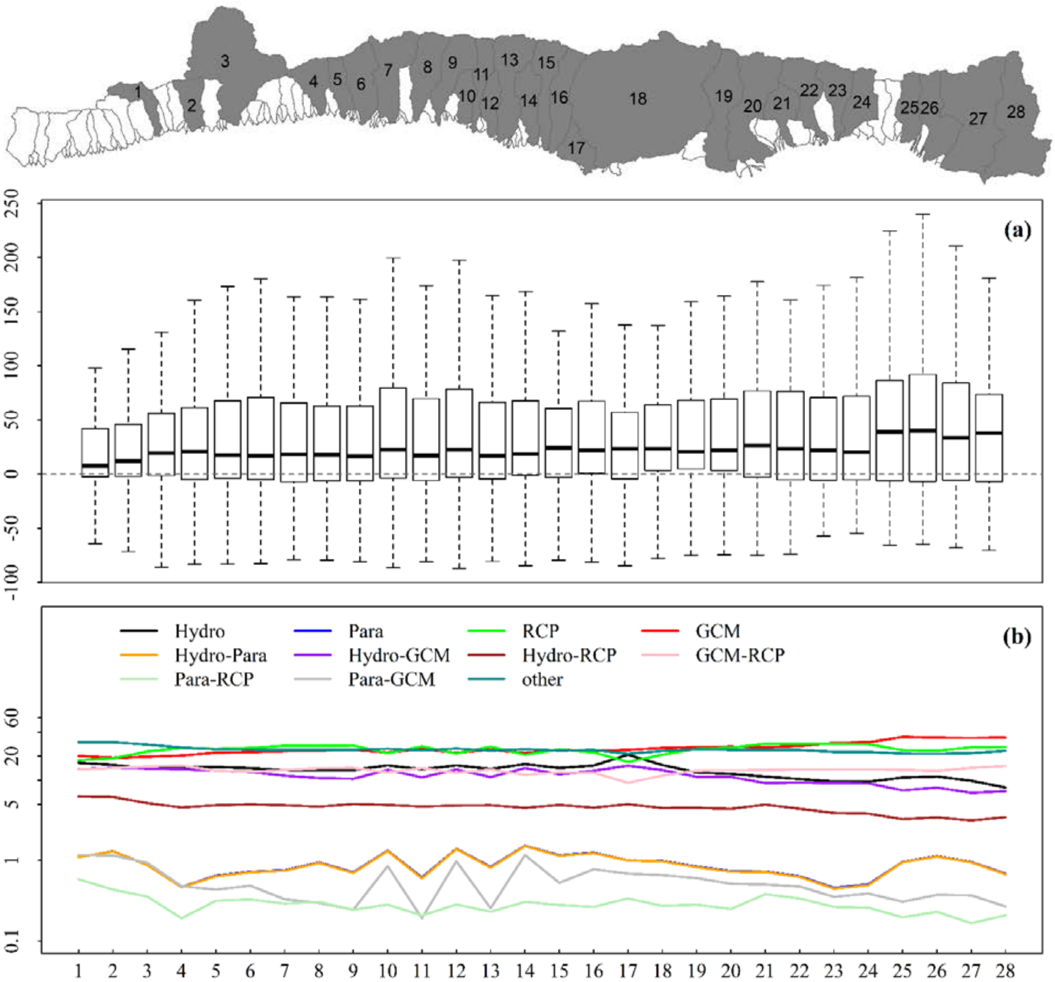

Figure 6. (a) Projected relative changes (%) in annual mean discharge (Q_p) in the major SBC watersheds (indicated by the grey watersheds in the map) during 2081-2100 as compared to historical period (1986-2005); each bar depicts relative changes in minimum, maximum, median, 1st and 3rd quartiles for the ensemble outputs; bars from left to right spatially corresponding to watersheds from west to east. For clarity, only watersheds with drainage areas larger than 7 km^2, which account for roughly 83% of the study area, are shown. (b) Relative sources (%) of the uncertainties in the projected changes at each of these watersheds; the category "other" is the uncertainty from the 3rd and 4th orders of interactions between the 4 major sources (i.e., GCMs, RCPs, Hydrologic models, denoted by "Hydro" and parameters denoted by "Para")

https://doi.org/10.5194/hess-2019-328
Preprint. Discussion started: 3 July 2019

Hydrology and Earth System Sciences
Open Access
Discussions

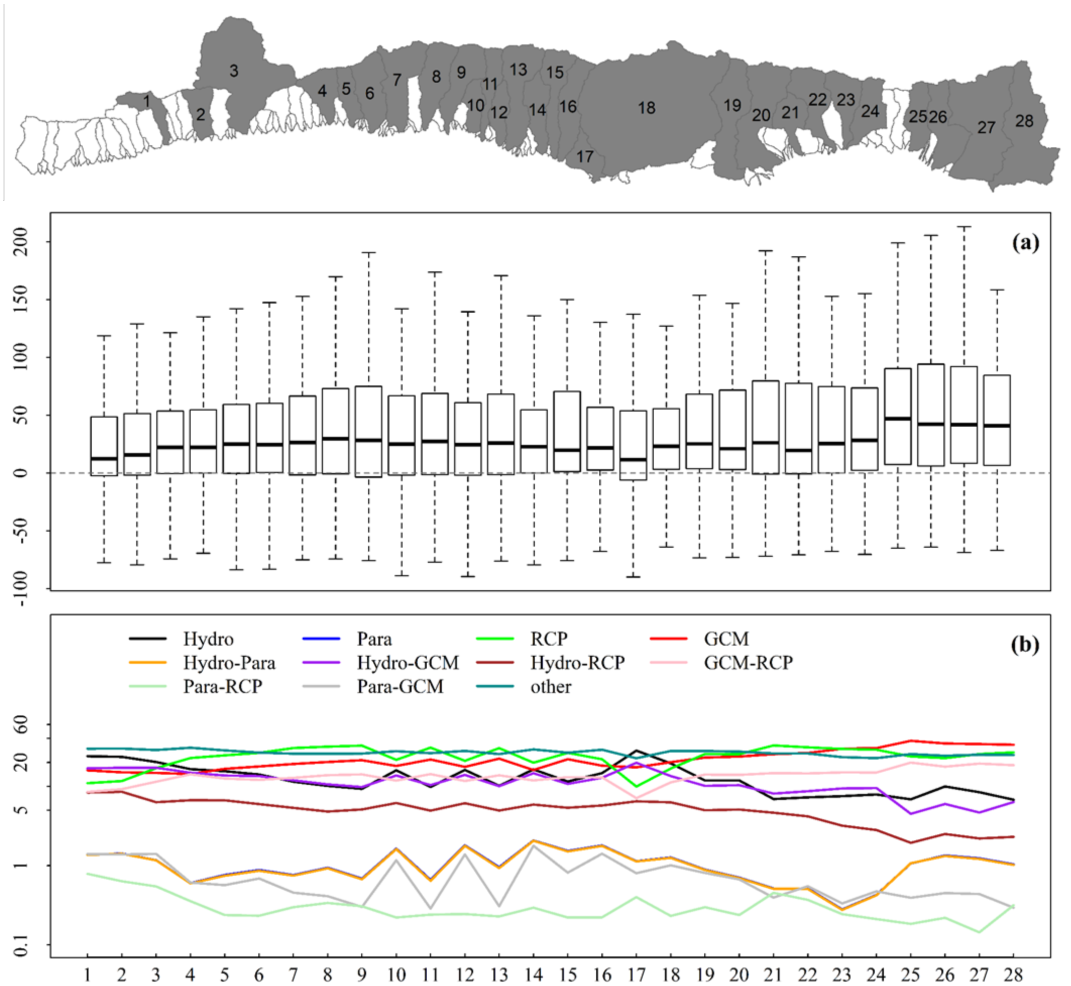

682 **Figure 7. (a) Projected relative changes (%) in 100-yr flood discharge (Q_{100}) in the major**
683 **SBC watersheds (indicated by the grey watersheds in the map) during 2081-2100 as**
684 **compared to historical period (1986-2005); each bar depicts relative changes in minimum,**
685 **maximum, median, 1st and 3rd quartiles for the ensemble outputs; bars from left to right**
686 **spatially corresponding to watersheds from west to east. For clarity, only watersheds with**
687 **drainage areas larger than 7 km^2, which account for roughly 83% of the study area, are**
688 **shown. (b) Relative sources (%) of the uncertainties in the projected changes at each of these**
689 **watersheds; the category "other" is the uncertainty from the 3rd and 4th orders of interactions**
690 **between the 4 major sources (i.e., GCMs, RCPs, Hydrologic models, denoted by "Hydro"**
691 **and parameters denoted by "Para")**

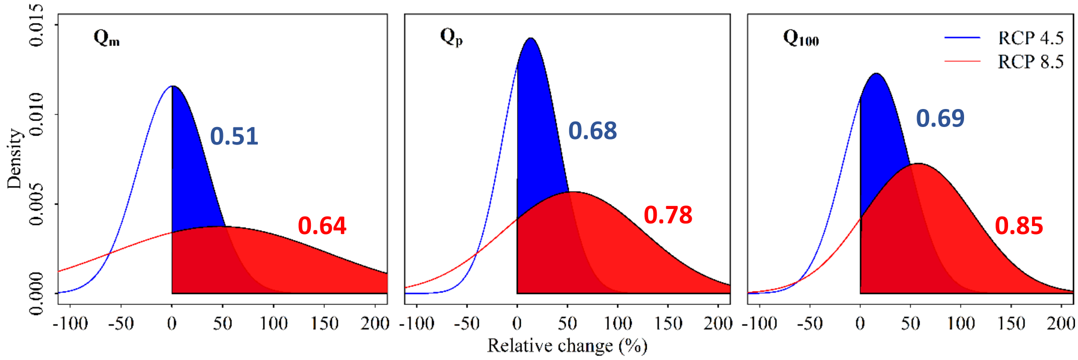

692 **Figure 8. Probability of changes in Q_m, Q_p and Q_{100} at Mission Creek watershed (No. 20 in**
693 **Figure 5 map). The numbers in the plot are the probabilities of positive changes in Q_m, Q_p**
694 **and Q_{100} (areas of shaded regions) under each emission scenario (blue numbers are for RCM**
695 **4.5 and red numbers are for RCP 8.5).**